Binding of Ca^{2+} to Glutamic Acid-Rich Polypeptides from the Rod Outer Segment

S. Haber-Pohlmeier,* K. Abarca-Heidemann,† H. G. Körschen,* H. Kaur Dhiman,‡ J. Heberle,§ H. Schwalbe,† J. Klein-Seetharaman,*†‡ U. B. Kaupp,* and A. Pohlmeier¶

*Institut für Neurowissenschaften und Biophysik, Forschungszentrum Jülich, Jülich, Germany; †J. W. Goethe Universität Frankfurt, Institut für Organische Chemie und Chemische Biologie, Center for Biomolecular Magnetic Resonance, Frankfurt, Germany; ‡Department of Structural Biology, University of Pittsburgh School of Medicine, Pittsburgh, Pennsylvania, USA; §Bielefeld University, Department of Chemistry Biophysical Chemistry (PC III), Bielefeld, Germany; and ¶ICG-IV, Forschungszentrum Jülich, Jülich, Germany

ABSTRACT Rod photoreceptors contain three different glutamic acid-rich proteins (GARPs) that have been proposed to control the propagation of Ca^{2+} from the site of its entry at the cyclic nucleotide-gated channel to the cytosol of the outer segment. We tested this hypothesis by measuring the binding of Ca^{2+} to the following five constructs related to GARPs of rod photoreceptors: a 32-mer peptide containing 22 carboxylate groups, polyglutamic acid, a recombinant segment comprising 73 carboxylate groups (GLU), GARP1, and GARP2. Ca^{2+} binding was investigated by means of a Ca^{2+}-sensitive electrode. In all cases, Ca^{2+} binds with low affinity; the half-maximum binding constant $K_{1/2}$ ranges from 6 to 16 mM. The binding stoichiometry between Ca^{2+} ions and carboxylic groups is ~1:1; an exception is GARP2, where a binding stoichiometry of ~1:2 was found. Hydrodynamic radii of 1.6, 2.8, 3.3, 5.7, and 6.7 nm were determined by dynamic light scattering for the 32-mer, polyglutamic acid, GLU, GARP2, and GARP1 constructs, respectively. These results suggest that the peptides as well as GARP1 and GARP2 do not adopt compact globular structures. We conclude that the structures should be regarded as loose coils with low-affinity, high-capacity Ca^{2+} binding.

INTRODUCTION

Glutamic acid-rich proteins (GARPs) exist in three forms in vertebrate rod photoreceptors (1–4). The GARP′ part represents the long N-terminal domain of the B1 subunit of the rod cyclic nucleotide-gated (CNG) channel, which interacts with peripherin, a tetraspanin protein at the rim of disks (5). There are two soluble isoforms of GARP′: GARP1, which is almost identical to the GARP′ part, and GARP2, which corresponds to the first 291 amino acids of GARP1, but lacks a region particularly rich in glutamic acid present in both the GARP′ and GARP1. This region is located between positions 355 and 465 in the bovine B1 subunit (2) and contains 68 glutamate and five aspartate residues (see Fig. 1). At physiological pH, the carboxylic groups of the acidic amino acids are almost completely deprotonated (vide infra) (6,7) and although some of the negative charge is compensated by 20 arginine and lysine residues, a significant surplus of negative charge is localized in a comparatively small space on this protein. A recent study of GARP proteins revealed that 89% of the GARP1 polypeptide exist in an unfolded conformation (8), i.e., GARPs belong to the class of intrinsically unstructured proteins (9,10). The high charge density has stimulated the hypothesis that the GARP′ region may serve as a low-affinity Ca^{2+} buffer that controls the Ca^{2+} dynamics inside the rod photoreceptor (1).

The aim of this work is to determine the affinity and stoichiometry for binding of Ca^{2+} to various glutamic acid-rich regions and to determine the hydrodynamic radii of the constructs. Together, the quantification of these properties allows one to estimate the maximum charge density and to derive the polyelectrolytic properties of these glutamic acid-rich peptides and the GARP proteins of the retina.

MATERIAL AND METHODS

Sample preparation

Polyglutamic acid and 32-mer peptide

Na^+-polyglutamic acid (PGA) (Sigma-Aldrich, Taufkirchen, Germany) has a mean molecular weight of $M_W = 7{,}700$, corresponding to a 51-mer. The 32-mer (EEKEDGEEEEEEGREKEEEEGEEKEEEEGREK), corresponding to amino acid residues 362–393 of the bovine B1 subunit, was custom synthesized (Biopeptide, San Diego, CA). Samples were dissolved in 0.15 M NaCl and 20 mM Tris/HCl; the pH was adjusted by NaOH or HCl.

Expression of the glutamic acid-rich region

The glutamic acid-rich region of GARP1 and GARP′ (GLU), consisting of 111 residues (amino acid residues 355–465 of the bovine B1 subunit), was obtained by heterologous expression (Fig. 2). This region contains 68 glutamate, five aspartate, 13 lysine, and seven arginine, 16 glycine, one valine, and one glutamine residues. For the expression in *Escherichia coli* cells (BL21 (DE3) pLysE) as Strep-tagged fusion protein, the gene was subcloned into the pASK-IBA vector (IBA, Göttingen, Germany). Cells were lysed by sonification (3 × 10 s) on ice in binding buffer (100 mM Tris/HCl at pH 8.0, 150 mM NaCl; 1 mM EDTA, complete protease inhibitor cocktail; Roche, Mannheim, Germany). Insoluble components were removed by centrifugation at 15,500 × *g* for 15 min at 4°C. The solubilized Strep-tagged GLU protein was purified using affinity chromatography (Strep-Tacin Sepharose column; IBA). After washing with 5 vol of binding buffer, the GLU protein was eluted in binding buffer containing 2.5 mM desthiobiotin. EDTA was removed to ≤0.1 mM by gel filtration using a NAP-5 minicolumn (GE Healthcare, Freiburg, Germany). The final concentration of GLU protein

Submitted August 6, 2006, and accepted for publication November 22, 2006.

Address reprint requests to S. Haber-Pohlmeier, INB-2, Forschungszentrum Jülich, 52425 Jülich, Germany. E-mail: s.haber-pohlmeier@fz-juelich.de.

0006-3495/07/05/3207/08 $2.00

doi: 10.1529/biophysj.106.094847

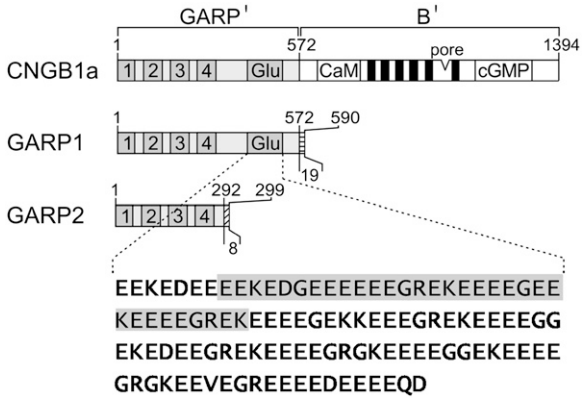

FIGURE 1 Schematic structures of the B1 subunit of the cyclic nucleotide-gated channel, GARP1, and GARP2. GARP′ represents the GARP part of B1, and B′ the channel part of the subunit. The amino-acid sequences of the glutamic acid-rich region (*GLU*) and 32-mer (highlighted in *gray*) are given below. (*R1–R4*) repeats; (*CaM*) calmodulin-binding site; (*black boxes*) transmembrane segments; (*cGMP*) cGMP-binding site.

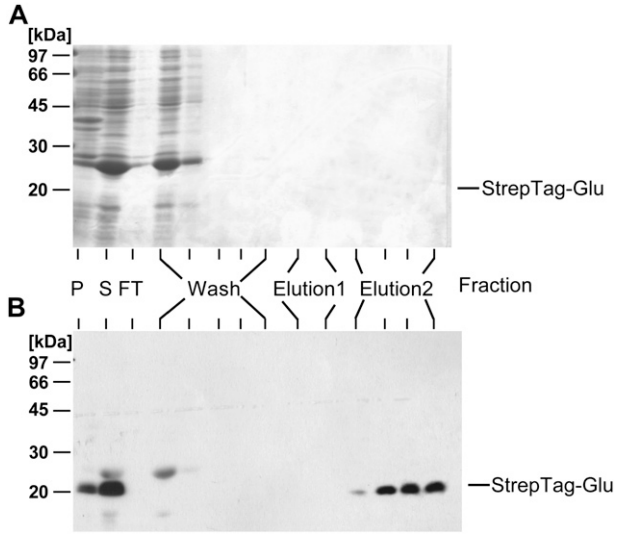

FIGURE 2 Purification of the glutamic acid-rich (*GLU*) domain of GARPs. (*A*) Coomassie-stained gel and (*B*) Western blot analysis of the GLU-containing fractions during the purification procedure. The Western blot analysis shown in panel *B* was performed using the monoclonal antibody Strep-tagII (IBA). On the left side of the gels, the M_w of the standard proteins are marked. Insoluble bacterial fraction (*P*), soluble fraction (*S*), flow-through (*FT*), elution fractions that do not contain GLU (*Elution1*), elution fractions that contain GLU (*Elution2*). Due to its high negative charge, the GLU domain does not bind the Coomassie blue dye and, therefore, is not visible in panel *A* as has been observed previously for GARP-related sequences (2–4). Note that flow-through contains less protein than first wash because of the small volume of cell lysate loaded compared to the column volume in this experiment.

was estimated by measuring the absorption at 280 nm (1.5 ± 0.5 mg/ml; $n = 5$), based on the extinction coefficient of tryptophan (5500 $M^{-1}cm^{-1}$) present in the Strep-tag sequence (WSHPQFEK).

Expression and purification of GARP1 and 2

Recombinant GARP1 and 2 were expressed in *E. coli* (BL21 (DE3) *pLysE* cells) as His-tagged fusion proteins using the pET30a vector (Novagen, Schwalbach, Germany). Cells were resuspended and lysed by sonication (3 × 10 s) in 10 mM Na^+ phosphate, pH 7.0. After addition of DNase (1000 units/l culture) and 2 mM $MgCl_2$, the suspension was incubated on ice for 15 min. Soluble recombinant GARPs were recovered by centrifugation (60,000 × *g*). The supernatant was adjusted to binding buffer A (20 mM Na^+ phosphate, pH 7.0, 35 mM imidazole, 2% v/v glycerol, and 500 mM NaCl) and loaded onto a $CoCl_2$-activated NTA-HiTrap column (Pharmacia/Pfizer, Karlsruhe, Germany). The column was washed with 10 vol of binding buffer A followed by 10 vol of binding buffer A containing 50 mM imidazole (GARP1) or 100 mM imidazole (GARP2). Recombinant GARPs were eluted with binding buffer A containing 500 mM imidazole. Further purification of GARP1 and GARP2 was performed by size-exclusion chromatography using a Sephacyl S-300 column or a Superdex 200 column (Pharmacia). GARP1- and GARP2-containing fractions were pooled and concentrated to 3 and 2.7 mg/ml, respectively, using Centriplus 30 and Centriplus 10 spin columns (Millipore, Schwalbach, Germany).

Expression and purification of GARP2 for NMR measurements

NMR experiments require milligram quantities of protein. Although such quantities can be obtained from the previously published *E. coli* expression system (8), this system requires growth of several liters of culture to obtain quantities suitable for NMR spectroscopy. We therefore also overexpressed GARP2 (amino-acid residues 1-274) as Strep-tagged fusion protein in *Sf9* cells using baculovirus infection. Baculovirus infection at a MOI8 for 72 h yielded 12 mg of GARP2 per liter of culture. Because of this high yield, growth of a single liter of culture provides sufficient material for NMR spectroscopy. Cells were lysed by homogenization on ice in binding buffer (100 mM Tris/HCl at pH 8.0, 150 mM NaCl; 1 mM EDTA, complete protease inhibitor cocktail) and soluble recombinant GARP2 was recovered by centrifugation (28,000 rpm; 40 min; 4°C). The Strep-tagged GARP2 protein was purified using affinity chromatography using a Strep-Tacin Sepharose column. The protein was eluted in binding buffer containing 2.5 mM desthiobiotin and concentrated to a final concentration of 0.1 mM for NMR experiments using a Centricon YM 10 tube (Millipore, Billerica, MA). The NMR spectra of GARP2 expressed in the baculovirus/Sf9 system (Fig. 5, *gray line*) were indistinguishable from those of GARP2 obtained from *E. coli* (8).

Ca^{2+}-binding isotherms

All buffers were purified by treatment with an ion-exchange column (Chelex-100, Na^+ form, Sigma-Aldrich Chemie, Munich, Germany) and all vessels were cleaned by washing with Chelex-100 treated water. The pH of buffers was controlled after Chelex-100 treatment. Small samples (0.15–0.5 ml) of the polypeptides in the respective buffers (see Table 1) have been titrated by addition of $CaCl_2$ from stock solutions in an Eppendorf vessel at constant temperature yielding total concentrations of $CaCl_2$ in the range between 7 μM and 0.05 M.

The activity of free Ca^{2+} was measured with a potentiometer (716-DMS-Titrino, Metrohm AG, Herisau, Switzerland) equipped with a Ca^{2+}-selective electrode (''detectION 041'' and a ''DRIREF-2'' reference electrode, WPI, Sarasota, FL). For each polypeptide or peptide sample, at least one calibration curve was determined under identical conditions. The calibration curve was fitted by the following empirical function:

$$\log\left([Ca^{2+}]_f\right) = Y_0 + mV - A\exp(-k(V - V_0)), \qquad (1)$$

wherein Y_0, m, A, k, and V_0 are fit parameters. $Y_0 + mV$ describes the Nernst relation between log ($[Ca^{2+}]_f$) and the voltage V; the term $A\exp(-k(V - V_0))$ takes into account the deviation from linearity for low $[Ca^{2+}]_f$. The absolute error of the electrode was estimated to be ±0.5 mV. This propagates into an uncertainty of log ($[Ca^{2+}]_f$) of ±0.02, i.e., $\Delta[Ca^{2+}]_f \approx \pm 5\%$.

TABLE 1 Summary of the results for PGA, the 32-mer, and the GLU region from the B1 subunit, and GARP1 and GARP2

Constructs		PGA*	PGA† + Ca^{2+}	32-mer*	32-mer† + Ca^{2+}	GLU‡	GLU§ + Ca^{2+}	GARP1‡	GARP2‡
No. of residues		51		32		111		590	299
No. of Asp + Glu residues		51		22		73		164	46
Maximum net charge¶		−51		−16		−53		−116	−25
DLS	$D°$ ($\mu m^2 s^{-1}$)‖	75 ± 3** (14)	80 ± 5** (14)	128 ± 8** (18)	140 ± 5†† (3)	54 ± 5†† (14)	60 ± 6†† (5)	27 ± 3†† (10)	30 ± 3†† (7)
	R_h (nm)	2.8 ± 0.1	2.7 ± 0.2	1.6 ± 0.1	1.4 ± 0.2	3.3 ± 0.3	3.0 ± 0.3	6.7 ± 1	5.7 ± 1
Titration	$K_{1/2}$ (mM)‡‡	16 ± 4 (3)		7 ± 2 (3)		6 (2)		10 ± 2 (3)	7 (2)
	n_{max}‡‡§§	0.8 ± 0.1 (3)		0.9 ± 0.1 (3)		1.0 (2)		0.8 ± 0.2 (3)	0.5 (2)

Fast translational diffusion coefficients ($D°$) and hydrodynamic radii (R_h) were derived from dynamic light scattering experiments; $K_{1/2}$ values and maximum binding ratios n_{max} from analysis of binding isotherms.

*0.02 M Tris, 0.15 M NaCl, pH = 7.2.

†0.02 M Tris, 0.15 M NaCl, pH = 7.2, 50 mM $CaCl_2$.

‡0.02 M Tris, 0.15 M NaCl, 5% glycerol, pH = 7.2.

§0.02 M Tris, 0.15 M NaCl, 5% glycerol, pH = 7.2, 20 mM $CaCl_2$.

¶Difference of anionic and cationic residues, assuming no binding of metal ions at pH = 7 without binding tags.

‖For each sample experiments have been performed at several angles (30–120°) and concentrations. Each experiment is the average of 10 single runs. The total number of experiments is noted in parentheses.

**Extrapolated to $c_P = 0$ according to Eq. 7; ''$\pm x$'' is the uncertainty calculated from the fit of Eq. 7; see Fig. 8.

††Obtained from measurements at very low concentrations, ''$\pm x$'' is mean ± SD.

‡‡Obtained from a fit of Eq. 4.

§§Maximum no. of bound Ca^{2+} ions per no. of Asp and Glu residues in the constructs including binding tags.

In practice, one has to consider an additional error of $\Delta\log[Ca^{2+}]_f = \pm 0.01$ caused by the uncertainty of the calibration curve. So the overall uncertainty of $[Ca^{2+}]_f$ is ~7%.

As an example, Fig. 3 shows the voltage V measured as function of the total $CaCl_2$ concentration for the calibration curve as well as for a solution containing 5 g/l PGA. The data were fitted by Eq. 1 and from this fit the concentration of free Ca^{2+} ($[Ca^{2+}]_f$) in the sample was calculated. The calibration curve deviated from linearity at $[Ca^{2+}]_f$ below ~30 μM; i.e., this value represents approximately the lowest concentration that can be determined by this procedure. The amount of bound Ca^{2+} ($[Ca^{2+}]_b$) was calculated according to:

$$[Ca^{2+}]_b = [Ca^{2+}]_t - [Ca^{2+}]_f. \quad (2)$$

The number of bound Ca^{2+} ions per carboxylic group residue was obtained from Eq. 3:

$$n_{Ca} = \frac{[Ca^{2+}]_b}{[RCOO^-]_t} = \frac{[Ca^{2+}]_b}{c_P(n_{Asp} + n_{Glu})/M_w}, \quad (3)$$

wherein n_{Asp} and n_{Glu} denote the number of aspartate and glutamate residues in the peptide, c_p is the peptide concentration, and M_w is the molecular weight. This quantity is plotted versus $[Ca^{2+}]_f$ in Fig. 4. The data were further analyzed by fitting to the binding isotherm:

$$n_{Ca} = n_{max}\frac{1/K_{1/2}[Ca^{2+}]_f}{1 + 1/K_{1/2}[Ca^{2+}]_f}, \quad (4)$$

wherein n_{max} refers to the maximal binding capacity and $K_{1/2}$ refers to the $[Ca^{2+}]_f$ at half-saturation. The state of protonation of PGA (1.5 mg/ml) was determined in 0.15 M NaCl electrolyte by titration with HCl. The titration curve had an inflection point at pH = 5.0 and reached a plateau for pH > 6.5. This provides evidence that the glutamate and aspartate residues in the constructs are deprotonated above pH 6.5.

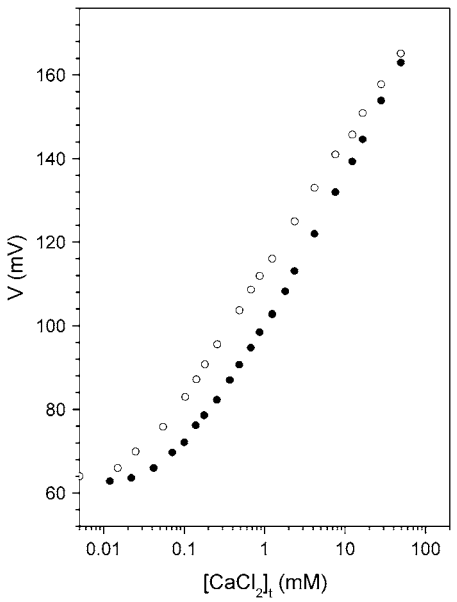

FIGURE 3 Determination of the free Ca^{2+} concentration with a Ca^{2+}-sensitive electrode at pH = 7.2 in 0.15 M NaCl solution. Measured voltages V in the absence (○) of peptide (*calibration curve*) and in the presence of 5 g/L Na-polyglutamate (●) at increasing total concentrations of $CaCl_2$. The size of the symbols corresponds approximately to the mean ± SD of 0.5 mV (five to six measurements).

Dynamic light scattering

Dynamic light-scattering measurements were performed with a device composed of an continuous wave Ar^+ laser operating at 488 nm, a goniometer, a photomultiplier/discriminator unit (SO-SIPD, ALV, Langen, Germany), and a correlator (ALV5000/E, ALV, Langen, Germany). Intensity autocorrelation functions $g_2(t)$ were recorded in vertical/vertical polarized geometry at scattering angles between 30° and 120° and temperatures ranging between 8°C and 20°C. Before the measurement, protein and peptide samples were

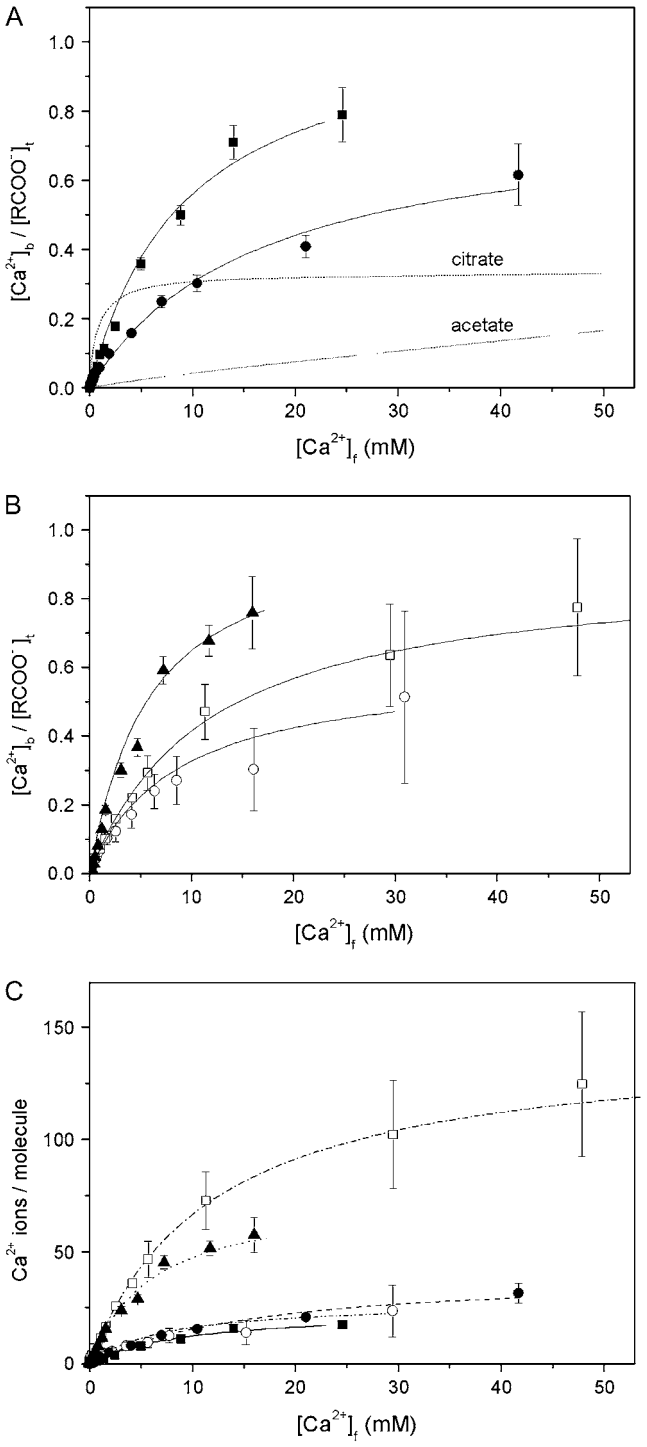

FIGURE 4 Ca^{2+} binding to five constructs as function of Ca^{2+} concentration. (*A*) Ca^{2+}-binding isotherms normalized to the total no. of acidic residues ($[Ca^{2+}]_b/[RCOO^-])_t$. 32-mer (■), and PGA (●). For comparison, calculated isotherms for the binding of Ca^{2+} to acetate and to citrate are also included. (*B*) Ca^{2+}-binding isotherms for GLU (▲), GARP1 (□), and GARP2 (○). The data represent the mean ± SD of two or three experiments (see Table 1). The continuous lines are fits of Eq. 4 to the data yielding values of $K_{1/2}$ and n_{max}. The error bars primarily result from the uncertainty of the determination of $[Ca^{2+}]_f$. (*C*) No. of bound Ca^{2+} ions per molecule, recalculated from panels *A* and *B*. Symbols used are identical to those in panels *A* and *B*.

filtered through 0.2 μm Anotop filters (WPI Inc. Sarasota, FL). The intensity autocorrelation functions of PGA and the 32-mer peptide were investigated in the concentration range between 3 and 20 mg/ml. The limited availability of the other polypeptides did not allow the determination of the concentration dependence.

Data analysis

The theory of dynamic light scattering is reviewed extensively in the literature (11). Therefore, only the basic equations are noted here. The normalized field-autocorrelation function $g_1(t)$ was calculated from the intensity autocorrelation function $g_2(t)$ by means of the Siegert relation ($g_2(t) = 1 + f(g_1(t))^2$), wherein f is the coherence factor. The distribution function $P(\Gamma)$ was derived from $g_1(t)$ according to:

$$g_1(t) = \int_{\Gamma_{min}}^{\Gamma_{max}} P(\Gamma)\exp(-\Gamma t)\, d\Gamma, \quad (5)$$

wherein Γ denotes the relaxation rate. Equation 5 was solved by means of regularization (12,13). The mean relaxation rate $\langle\Gamma\rangle$ of one mode of the distribution function is related to the apparent translational diffusion coefficient D by

$$D = \langle\Gamma\rangle/q^2, \quad (6)$$

wherein q is the scattering vector. Weak linear relations have been observed between D and the concentration of the polypeptides or peptides c_P, which allowed the calculation of the diffusion constant at infinite dilution, $D°$, according to

$$D = D°(1 + k_v c_P), \quad (7)$$

wherein k_v is the empirical second virial coefficient. The zero-concentration diffusion constant $D°$ can be related to the hydrodynamic radius R_H by the Stokes-Einstein equation for an equivalent sphere according to

$$R_H = k_B T/(6\pi\eta D°), \quad (8)$$

wherein k_B is the Boltzmann constant, T the absolute temperature, and η the viscosity of the solvent.

RESULTS AND DISCUSSION

Binding isotherms

The binding of Ca^{2+} to the five GARP constructs was determined by measuring the concentration of free Ca^{2+} using Ca^{2+}-sensitive electrodes (Fig. 3). The corresponding Ca^{2+}-binding isotherms are shown in Fig. 4 and the results are summarized in Table 1. The binding isotherms were normalized with respect to the number of carboxylate residues in each case to allow comparison among constructs (Fig. 4, *A* and *B*). For comparison, the nonnormalized data are shown in Fig. 4 *C*. From fitting of the binding isotherm (Eq. 4) to the experimental data, values for $K_{1/2}$ and n_{max} were obtained.

The Ca^{2+}-binding isotherm of PGA (5 g/l) (Fig. 4 *A*) yielded a $K_{1/2} = 16$ mM and a $n_{max} = 0.8$ (Table 1). High-affinity binding sites were not observed. The corresponding values for the 32-mer were $K_{1/2} = 7$ mM and $n_{max} = 0.9$ (Fig. 4 *A*; Table 1); i.e., the 32-mer binds Ca^{2+} with slightly higher affinity than PGA whereas the binding capacity is similar. This difference might result from the higher electrostatic potential inside the more compact coil of the 32-mer.

The Ca^{2+}-binding isotherms of GLU, GARP1, and GARP2 are shown in Fig. 4 *B*, and the results are summarized in Table 1. All constructs by and large have a similar affinity and binding capacity for Ca^{2+}, with the exception of GARP2, whose capacity is roughly half (Fig. 4, *A* and *B*). In conclusion, the constructs are low-affinity and high-capacity buffers for Ca^{2+}, and the absolute number of Ca^{2+} ions bound per construct is largest for GARP1 due to its higher content of carboxylate residues (Fig. 4 *C*).

NMR spectroscopy of GARP2

NMR experiments were performed to further characterize the binding of Ca^{2+} to GARP2. Ca^{2+}-induced conformational changes or coordination of Ca^{2+} through a well-defined binding pocket such as is observed in high-affinity Ca^{2+} -binding proteins (e.g., calmodulin) should lead to a change in the chemical shifts of the protein. Proton one-dimensional (1D) type experiments were recorded on a 600-MHz Bruker spectrometer at 298 K in elution buffer (binding buffer + 2.5 mM Desthiobiotin)/10% D_2O with a protein concentration of 0.1 mM. The addition of 5 mM Ca^{2+} did not change the protein amide signals (Fig. 5 *B*), indicating that Ca^{2+} does not induce large conformational changes such as those observed in calmodulin and that Ca^{2+} binding does not occur through structurally well-defined binding pockets in this protein.

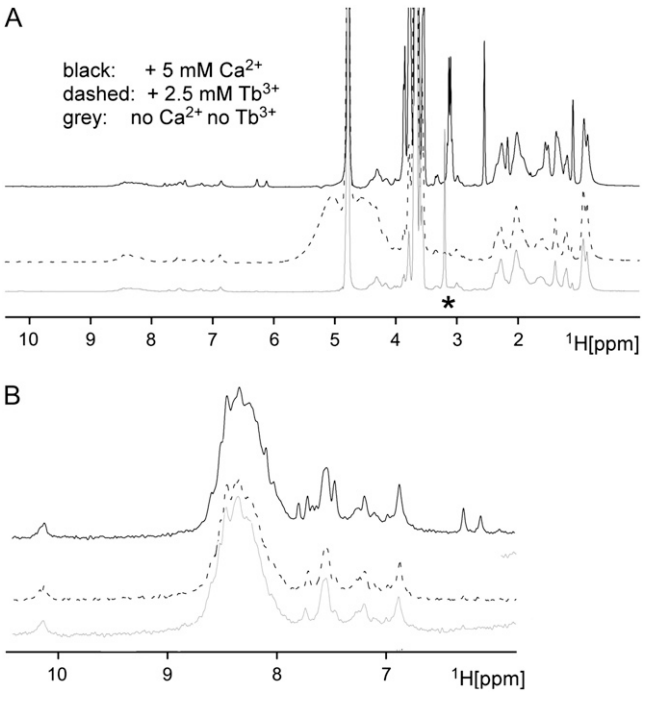

FIGURE 5 One-dimensional ^1H NMR spectra of GARP2. (*A*) One-dimensional ^1H NMR spectra of GARP2 with or without $Ca^{2+}$and Tb^{3+}. (*B*) 1D ^1H NMR spectra showing the amide region of GARP2 with or without Ca^{2+} and Tb^{3+}. Spectra were acquired at 298 K in a buffer containing 100 mM Tris pH 8.0, 150 mM NaCl, 1 mM EDTA, 2.5 mM desthiobiotin before and after adding 5 mM Ca^{2+} or Tb^{3+}. The protein concentration was 0.1 mM. The asterisk shows the EDTA signals.

To confirm the presence of binding sites, Tb^{3+} was added. Tb^{3+} acts as a paramagnetic substitute for Ca^{2+} in this experiment and should lead to broadening of the NMR signals if it interacts with the protein. When Tb^{3+} was added to the protein, the signals of the side chains became attenuated (Fig. 5, *A* and *B*, *dashed spectra*). This observation supports the conclusion that ionic attraction of Tb^{3+} through the high negative charge density of GARP2 results in close proximity of Tb^{3+}, and by inference Ca^{2+}, to the amino acid residues of the protein.

Dynamic light scattering

To determine the hydrodynamic size of the constructs, we have performed dynamic light-scattering experiments at different scattering angles, temperatures, and concentrations. Fig. 6 *A* shows typical intensity correlation functions for the 32-mer, PGA, GLU, GARP1, and GARP2 at a scattering angle of 90° and $T = 20°C$. The functions decreased rapidly for the 32-mer and PGA, but a significantly slower decay was observed for GLU, GARP1, and GARP2.

The correlation functions have been further analyzed by determining the corresponding distributions of relaxation rates (Fig. 6 *B*). Bimodal distributions were observed for all samples. For the 32-mer and PGA, the areas under the two mode peaks were similar, which reflects similar amplitudes of the autocorrelation functions in Fig. 6 *A*. In contrast, the slow mode dominated the spectra of GLU, GARP1, and GARP2. From these distribution functions, mean relaxation rates were calculated for the fast (Γ_f) and the slow (Γ_s) modes. They were analyzed further with respect to their angular and concentration dependence. Equation 6 predicts a linear relationship between relaxation rate Γ and scattering vector q^2 for the diffusion of particles. This holds true for the fast modes Γ_f of PGA and GLU (Fig. 7, *A* and *B*) and also for the 32-mer, GARP1, and GARP2 (data not shown). In contrast, the slow modes Γ_s were characterized by a significant deviation from linearity.

A bimodal behavior is frequently observed for polyelectrolytes in solution and the nature of the modes has been intensively studied. The fast mode is due to diffusion of individual polymer molecules at high ionic strength. Slow modes can arise either from aggregation of individual polymer chains or from hydrodynamic and electrostatic interactions between them (14–16). For the purpose of this work, only the size of individual polymer chains is significant; therefore, further consideration of the slow mode is omitted. It should be noted that the previously observed presence of mixtures of monomeric and oligomeric states of GARPs (8) is confirmed in this study.

We determined the diffusion coefficients $D°$ and the corresponding hydrodynamic radii for the monomers by measuring the concentration dependence of the fast diffusion

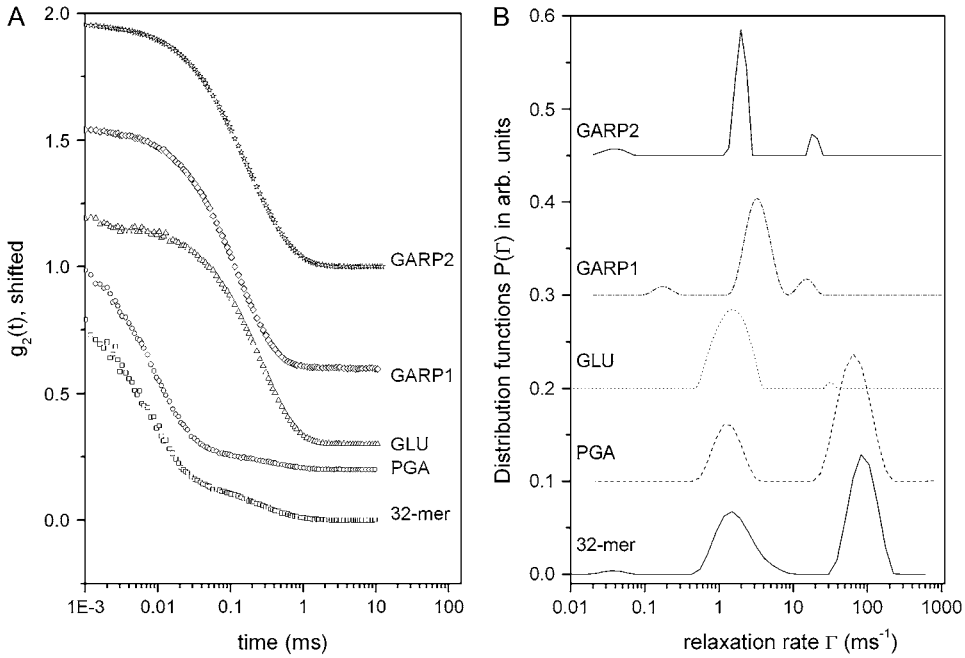

FIGURE 6 Light-scattering experiments. (*A*) Intensity autocorrelation functions $g_2(t)$ for various peptides and proteins at a scattering angle of 90° and $T = 20°C$. The functions are shifted along the ordinate for clarity. The concentrations are: 32-mer, 14 g/L; PGA, 17 g/L; GLU, 1.5 g/L; GARP1, 3 g/L; GARP2, 2.7 g/L. (*B*) Inverse Laplace transforms (Eq. 5) of the autocorrelation functions in panel *A*, recalculated into field autocorrelation functions.

coefficient D_{fast}, shown in Fig. 8 for PGA and the 32-mer. As expected from Eq. 7, linear relations were observed, and the resulting diffusion coefficients $D°$ for the monomers are summarized in Table 1. For the other constructs, $D°$ was determined from D_{fast} at very low concentrations; see also Fig. 8. From $D°$, the hydrodynamic radii for equivalent spheres were calculated according to Eq. 8. Hydrodynamic radii of 1.6, 2.8, 3.3, 5.7, and 6.7 nm were obtained for the 32-mer, PGA, GLU, GARP2, and GARP1 constructs, respectively. It was observed that the addition of Ca^{2+} in high amounts leads to a small decrease of the hydrodynamic radii by 0.1–0.3 nm; see also Table 1.

The determined radii are consistent with intrinsically unstructured or extended conformations. First, the distribution functions of relaxation rates observed for PGA and the 32-mer are similar to those observed for synthetic polyelectrolytes such as poly(methacrylic acid) and poly(styrenesulfonate) that exist as random coils (14,16). Second, if PGA and the 32-mer would exist as compact coils, hydrodynamic radii of ~1.4 nm and 1.2 nm, respectively, are expected

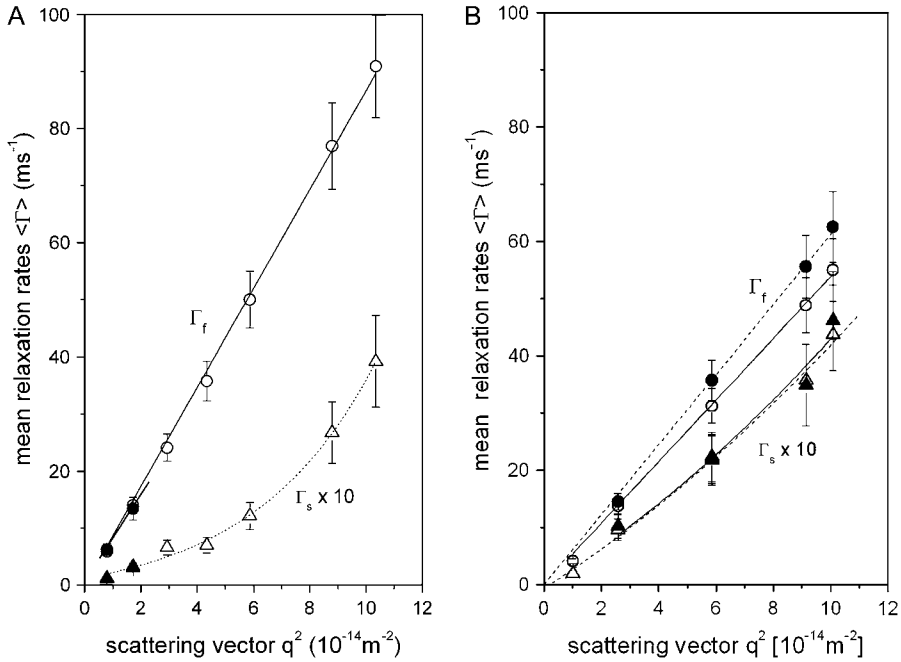

FIGURE 7 Angular (q) dependence of the mean fast and slow relaxation rates. (*A*) PGA (5 g/L) and (*B*) 1.5 g/L GLU. The buffer composition is given in Table 1. Open symbols refer to measurements without $CaCl_2$ and solid symbols to measurements in the presence of $CaCl_2$ (see Table 1). (○, ●) Fast relaxation rates Γ_f; (△, ▲) slow relaxation rates Γ_s. The straight lines are fits of Eq. 6 to Γ_f yielding $D_f = 87 \pm 5$ $\mu m^2 s^{-1}$ and 80 ± 8 $\mu m^2 s^{-1}$ for PGA without and with $CaCl_2$, respectively. For GLU, $D_f = 54 \pm 5$ and 60 ± 6 $\mu m^2 s^{-1}$, respectively.

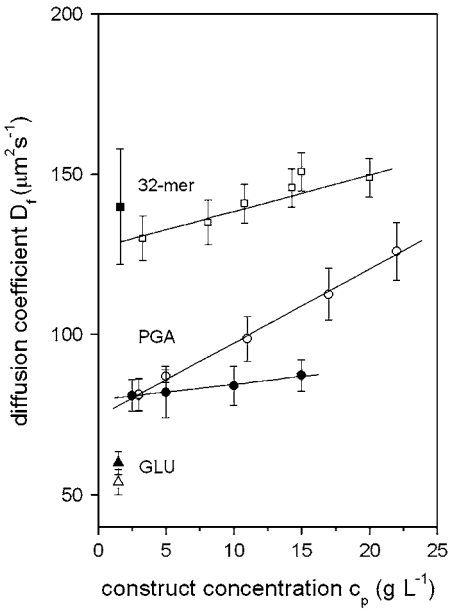

FIGURE 8 Dependence of the fast diffusion mode D_f on the concentration of the 32mer (□), PGA (○), and PGA with 50 mM Ca^{2+} (●). Buffer compositions are given in Table 1. The lines are fits of Eq. 7. Values obtained for D_f at one concentration of the 32-mer with 50 mM Ca^{2+} (■), GLU without Ca^{2+} (△), and GLU with 20 mM Ca^{2+} (▲) are also shown.

assuming a partial molecular volume of ~0.65 cm^3/mol and a value of $\delta_{H_2O} \cong 0.34$ g/g (17). Third, PGA, GARP1, and GARP2 have all been shown by independent methods to exist at neutral pH in an unstructured conformation (8,18).

CONCLUSIONS

Here, we show that various constructs derived from glutamic acid-rich proteins of rod outer segments display hydrodynamic sizes consistent with intrinsically unstructured proteins and bind Ca^{2+} with low affinity but high capacity. These properties are in par with other known cellular Ca^{2+} buffers that contain low-affinity Ca^{2+}-binding sites, such as the 40-kDa basement-membrane glycoprotein (19), γ-carboxyglutamate, a synthetic model for protein C (20), and calsequestrin (21). Particularly striking is the similarity to hyalin, a protein with a high content of random coil and 700 acidic residues, which contains Ca^{2+}-binding sites with $K_{1/2} \cong 1.5$ mM (22). Although Ca^{2+} binding to the GARP construct studied results in a slight compaction as evidenced by dynamic light scattering, it does not result in large conformational changes that would be detectable with NMR spectroscopy.

Why does the rod outer segment need loose coils of polymers that weekly bind Ca^{2+}? The small hydrodynamic volumes of GARPs create a rather high charge density in their coil interior resulting in a considerable enrichment of Ca^{2+}. However, the charge densities are not high enough to promote counterion condensation, because the minimum mean separation of two charges is larger than the Bjerrum length (23). Thus, the affinity of the construct for Ca^{2+} is stronger than that of single carboxylates, but much weaker than the high-affinity Ca^{2+}-binding sites such as found in calmodulin. GARPs, apart from their role to maintain the structure of the stack of disks (24), may serve two additional functions. First, GARPs may act as efficient Ca^{2+} buffers where Ca^{2+} can become available whenever it is needed during the photoreceptor adaptation process that is known to be regulated at numerous sites by Ca^{2+} (25). The buffering capacity of GARPs will depend on how much Mg^{2+} is competing with Ca^{2+} for the glutamate residues. More importantly, the GARP part of the CNG channel may function as a molecular wire that is ''channeling'' Ca^{2+} from the exit site of channel onto the surface of the disk (1) and thereby compartmentalizes Ca^{2+} microdomains.

We are grateful to N. Jordan for the preparation of *E. coli* GARP1 and GARP2, to Dr. D. Tränkner for initial help with the Ca^{2+} measurements, and to Dr. J. Woehnert for helpful discussions related to the NMR measurements.

The authors thank the Deutsche Forschungsgemeinschaft (PO 746/1 and KA 545/8-3) and the Sofya Kovalevskaya Award (to JKS) by the Humboldt-Foundation and the Zukunftsinvestitionsprogramm der Bundesregierung Deutschlands for financial support.

REFERENCES

1. Kaupp, U. B., and R. Seifert. 2002. Cyclic nucleotide-gated ion channels. *Physiol. Rev.* 82:769–824.
2. Körschen, H. G., M. Illing, R. Seifert, F. Sesti, A. Williams, S. Gotzes, C. Colville, F. Müller, A. Dosé, M. Godde, L. Molday, U. B. Kaupp, and R. S. Molday. 1995. A 240 kDa protein represents the complete β subunit of the cyclic nucleotide-gated channel from rod photoreceptor. *Neuron.* 15:627–636.
3. Körschen, H. G., M. Beyermann, F. Müller, M. Heck, M. Vantler, K.-W. Koch, R. Kellner, U. Wolfrum, C. Bode, K. P. Hofmann, and U. B. Kaupp. 1999. Interaction of glutamic-acid-rich proteins with the cGMP signalling pathway in rod photoreceptors. *Nature.* 400:761–766.
4. Colville, C. A., and R. S. Molday. 1996. Primary structure and expression of the human β-subunit and related proteins of the rod photoreceptor cGMP-gated channel. *J. Biol. Chem.* 271:32968–32974.
5. Poetsch, A., L. L. Molday, and R. S. Molday. 2001. The cGMP-gated channel and related glutamic acid-rich proteins interact with peripherin-2 at the rim region of rod photoreceptor disc membranes. *J. Biol. Chem.* 276:48009–48016.
6. Wada, A. 1960. Helix-coil transformation and titration curve of poly-L-glutamic acid. *Mol. Phys.* 3:409–416.
7. Martell, A. E., and R. M. Smith. 1977. Critical Stability Constants. Plenum Press, New York.
8. Batra-Safferling, R., K. Abarca Heidemann, H. G. Körschen, C. Tziatzios, M. Stoldt, I. Budyak, D. Willbold, H. Schwalbe, J. Klein-Seetharaman, and U. B. Kaupp. 2005. Glutamic acid-rich proteins of rod photoreceptors are natively unfolded. *J. Biol. Chem.* 281:1449–1460.
9. Dyson, H. J., and P. E. Wright. 2005. Intrinsically unstructured proteins and their functions. *Nat. Rev. Mol. Cell Biol.* 6:197–208.
10. Tompa, P. 2002. Intrinsically unstructured proteins. *Trends Biochem. Sci.* 27:527–533.
11. Schmitz, K. S. 1990. Introduction to Dynamic Light Scattering by Macromolecules. Academic Press, Boston, MA.

12. Provencher, S. W. 1982. A constrained regularization method for inverting data represented by linear algebraic or integral equations. *Comp. Phys. Comm.* 27:213–227.

13. Provencher, S. W. 1982. Contin: a general purpose constrained regularization program for inverting noisy linear algebraic and integral equations. *Comp. Phys. Comm.* 27:229–242.

14. Pohlmeier, A., and S. Haber-Pohlmeier. 2004. Ionization of short polymethacrylic acid: titration, DLS, and model calculations. *J. Coll. Interf. Sci.* 273:369–380.

15. Sedlak, M. 2002. Generation of multimacroion domains in polyelectrolyte solutions by change of ionic strength or pH (macroion charge). *J. Chem. Phys.* 116:5256–5262.

16. Sedlak, M. 2001. Structure and dynamic of polyelectrolyte solutions by light scattering. *In* Physical Chemistry of Polyelectrolytes. T. Radeva, editor. Marcel Dekker, New York. 1–58.

17. Cantor, C. R., and P. R. Schimmel. 1980. Ultracentrifugation. *In* Biophysical Chemistry, Part II. Freeman, New York. 591–641.

18. Nilsson, S., and W. Zhang. 1990. Helix-coil transition of a titrating polyelectrolyte analyzed within the Poisson-Boltzmann cell model: effects of pH and salt concentration. *Macromolecules.* 23: 5234–5239.

19. Maurer, P., U. Mayer, M. Bruch, P. Jeno, K. Mann, R. Landwehr, J. Engel, and R. Timpl. 1992. High-affinity and low-affinity calcium binding and stability of the multidomain extracellular 40-kDa basement membrane glycoprotein (BM-40/SPARC osteonectin). *Eur. J. Biochem.* 205:233–240.

20. Colpitts, T. L., and F. J. Castellino. 1994. Calcium and phospholipid-binding properties of synthetic gamma-carboxyglutamic acid-containing peptides with sequence counterparts in human protein C. *Biochemistry.* 33:3501–3508.

21. Mitchell, R. D., H. K. B. Simmerman, and L. R. Jones. 1988. Ca^{2+} binding effects on protein conformation and protein interactions of canine cardiac calsequestrin. *J. Biol. Chem.* 263:1376–1381.

22. Rimsay, R., and J. J. Robinson. 2003. Biochemical analysis of hyalin gelation: an essential step in the assembly of the sea urchin extraembryonic matrix; the hyaline layer. *Arch. Biochem. Biophys.* 414: 279–286.

23. Manning, G. S., and J. Ray. 1998. Counterion condensation revisited. *J. Biomol. Struct. Dyn.* 16:461–476.

24. Huttl, S., S. Michalakis, M. Seeliger, D.-G. Luo, N. Acar, H. Geiger, K. Hudl, R. Mader, S. Haverkamp, M. Moser, A. Pfeifer, A. Gerstner, et al. 2005. Impaired channel targeting and retinal degeneration in mice lacking the cyclic nucleotide-gated channel subunit CNGB1. *J. Neurosci.* 25:130–138.

25. Baehr, W., and K. Palczewski. 2003. Photoreceptors and Calcium. Springer, London, UK.